ISSN 0021-8944, Journal of Applied Mechanics and Technical Physics, 2020, Vol. 61, No. 1, pp. 14–24. © Pleiades Publishing, Ltd., 2020.
Original Russian Text © G.S. Yan'kova, A.A. Cherevko, A.K. Khe, O.B. Bogomyakova, A.A. Tulupov.

STUDY OF HYDROCEPHALUS USING POROELASTIC MODELS

G. S. Yan'kova[a,b], A. A. Cherevko[a,b], A. K. Khe[a,b,*], O. B. Bogomyakova[c], and A. A. Tulupov[b,c]

UDC 51-76; 519.63

Abstract: The filtration of arterial, venous, and capillary blood, and liquor is investigated using a multiphase poroelastic model for brain matter based on medical data. The model can be used to describe the healthy brain, the brain with hydrocephalus, and the transition between them due to a change in model parameters.

Keywords: mathematical modeling, poroelasticity, cerebrospinal fluid, hydrocephalus.

DOI: 10.1134/S0021894420010022

INTRODUCTION

One of the processes specific to the brain is the flow of cerebrospinal fluid (CSF, liquor), which is a clear fluid whose density and viscosity are close to those of water.

CSF fills the ventricles of the brain and the subarachnoid spaces of the brain and the spinal cord. CSF flow in the intracranial cavity and the spinal canal has a complex pulsating character and is associated with cardiac activity [1, 2].

Various diseases of the central nervous system change the dynamics of liquid media of the central nervous system (CNS), which, in turn, may lead to changes in the brain. For example, in hydrocephalus, the ventricles of the brain are increased, resulting in displacement and compression of the brain tissue. This condition is well described in terms of clinical manifestations, but its causes and development are not well understood.

One of the main methods for the intravital study of the human liquor system is magnetic resonance imaging (MRI) used for non-invasive quantitative and qualitative assessment of the dynamics of liquor circulation both in norm and in pathology. MRI can be used to visualize CSF flow and quantitatively evaluate its velocity and the structural state of brain matter [3]. Intracranial pressure, which can only be measured invasively, is also of great importance.

Since the current level of medicine does not allow the long-term and continuous acquisition of data on cerebral processes, researchers and practitioners are forced to put forward various hypotheses about the mechanisms of interaction between the CNS divisions. Since these hypotheses have not yet been able to provide an understanding of the causes and mechanisms of the formation and development of hydrocephalus, it is advisable to use mathematical modeling to study this pathological condition.

[a]Lavrent'ev Institute of Hydrodynamics, Siberian Branch, Russian Academy of Sciences, Novosibirsk, 630090 Russia; galinayankova2703@gmail.com; cherevko@mail.ru; *alekhe@hydro.nsc.ru. [b]Novosibirsk State University, Novosibirsk, 630090 Russia. [c]International Tomographic Center, Siberian Branch, Russian Academy of Sciences, Novosibirsk 630090, Russia; bogom_o@tomo.nsc.ru; taa@tomo.nsc.ru. Translated from Prikladnaya Mekhanika i Tekhnicheskaya Fizika, Vol. 61, No. 1, pp. 17–29, January–February, 2020. Original article submitted July 12, 2019; revision submitted July 12, 2019; accepted for publication September 30, 2019.

*Corresponding author.

In the literature, there are several basic approaches to the mathematical modeling of intracranial hydrodynamics, including in hydrocephalus. The first approach uses compartmental models such as pressure–volume ($P-V$) models, which depend only on time and electrical circuit models [4–8]. The second approach uses models that depend on time and space such as poroelastic [9–12] or viscoelastic [13–15] models. In addition, in studies of the brain with hydrocephalus, methods of computational fluid dynamics (CFD) and CFD simulation are used [16–20]. These methods allow the study of velocity and pressure fields which cannot be investigated using medical imaging techniques.

In the present study of the development of hydrocephalus, we use a poroelastic model.

1. CEREBROSPINAL FLUID FLOW IN THE CRANIAL CAVITY. THE OCCURRENCE OF HYDROCEPHALUS

It is believed that CSF is secreted through the epithelium of the vascular plexuses in all four ventricles of the brain. Further liquor circulates from two lateral ventricles to the third ventricle through Monroe's foramen (interventricular foramen) and then along the third ventricle and passes through the Sylvian aqueduct. After that, CSF moves into the fourth ventricle and passes through Magendie's and Luschka's foramens into the subarachnoid space of the brain and spinal cord. Further, liquor is absorbed in the venous sinuses through the arachnoid granulations (Fig. 1).

Liquor not only fills the ventricles and surrounds the brain, but also seeps into brain tissue [is interstitial (intercellular) fluid], passing through the permeable walls of the lateral ventricles and filling the entire intercellular space of the brain.

The volume of CSF in humans varies with age, which is due to a change in the volume of the ventricular system: it is 15–20 ml in a newborn infant, 35 ml in a one-year-old child, 60–80 ml in a 5-year-old child, 100–200 ml in a 10-year-old child, and up to 140 ml in an adult. Within 24 hours, fluid can be exchanged 3–4 times in an adult and up to 6–8 times in infants [21].

Hydrocephalus is a pathology characterized by excessive accumulation of CSF in the ventricular system of the brain due to impairment of CSF flow from the site of secretion (cerebral ventricles) to the site of absorption into the blood circulatory system or as a result of a disturbance of absorption. Clinically, hydrocephalus manifests itself, first of all, in the form of a headache and a change in mental status. In children, hydrocephalus can lead to an increase in head size, and in elderly people, to a loss of bladder control [22].

In hydrocephalus, an the cerebral ventricles are increased, indicating an increased pressure in them (Fig. 2). In some cases, the increase in ventricular volume may be insignificant.

Treatment of hydrocephalus is primarily based on the diversion of excess CSF in such a way as to alleviate the symptoms of the disease. This is usually achieved by surgery.

Nevertheless, the CSF flow dynamics after treatment is not identical to that in the normal condition. Both the normal and pathological dynamics of CSF are poorly understood. Any additional information contributes to the development of strategies of medical intervention to normalize CSF flow in the case of hydrocephalus.

2. MATHEMATICAL MODELING OF INTRACRANIAL DYNAMICS

One approach to modeling intracranial hydrodynamics is to use lumped-parameter models or compartmental models. In these models, the intracranial contents is represented in the form of interconnected compartments, among which fluid exchange occurs [23–25]. Such models are a system of coupled ordinary differential equations describing the evolution of fluid pressure in each compartment. Solution of this system provides the relationship between intracranial pressure and the volume of the ventricles (see, e.g., [26]). This pressure–volume relation is used for diagnostics and treatment of hydrocephalus, but the main disadvantage of this approach is that spatial changes are not considered for any physical parameter, making it impossible to describe the stress and strain distributions in brain tissue or predict the fluid distribution in hydrocephalus. These significant limitations have led in the last decade to switching from lumped-parameter models to more realistic spatial models of the brain in hydrocephalus. This marked the beginning of the development of a biomechanical approach to modeling hydrocephalus. Hakim [27]

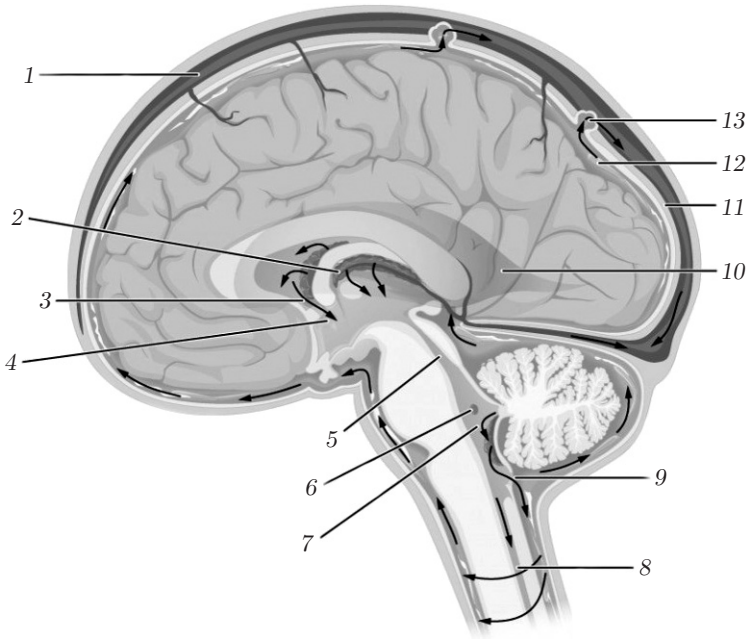

Fig. 1. Cerebrospinal fluid circulation (see https://radiografia.info): (*1*) superior sagittal sinus; (*2*) vascular plexus; (*3*) interventricular foramen; (*4*) third ventricle; (*5*) Silvyan aqueduct; (*6*) Luschka's foramen (lateral foramen of the fourth ventricle); (*7*) fourth ventricle; (*8*) central spinal canal; (*9*) Magendie's foramen (medial foramen of the fourth ventricle); (*10*) right lateral ventricle; (*11*) dura mater; (*12*) subarachnoid space; (*13*) arachnoid granulation.

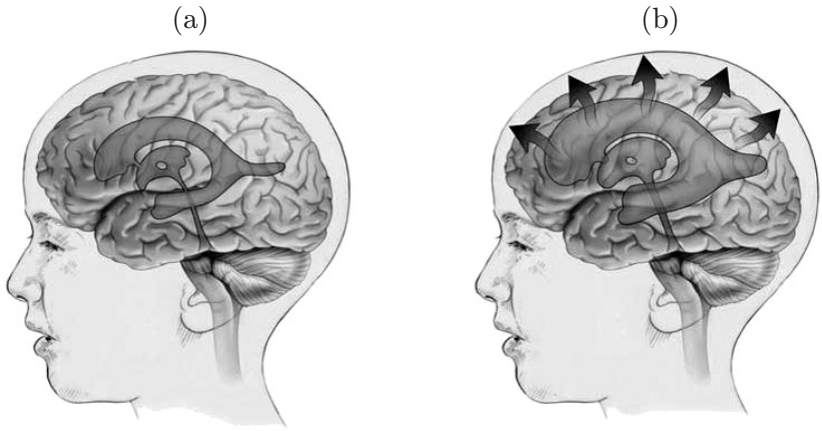

Fig. 2. Brain with normal ventricles (a) and enlarged ventricles in hydrocephalus (b); see https://neuromed.online.

was the first to use the three-dimensional (spherical) geometry of the brain and takes into account the porosity of the brain and its response to an enlargement of cerebral ventricles. It is assumed that the parenchyma material consists of an elastic matrix (neurons and neuroglia), whose pores are filled with CSF. The liquid phase flows inside the matrix under a pressure gradient.

In [9] this concept was formalized in terms used in the Biot poroelastic theory and the finite element method (FEM). Applying the FEM to a two-dimensional system consisting of ventricles surrounded by the porous brain, Nagashima et al. [9] calculated the pressure and strain distributions in the brain as a result of ventricular dilatation. They used the real geometry of the human ventricular system obtained from MRI data.

Pena [28] developed a linear poroelastic model [9] in studying the process of ventricular dilatation depending on time. This model was used to evaluate the compression and dilatation regions, which provided a better understanding of the stress concentration and the anatomy of the ventricles. In addition, the model [28] can be used to examine the leak of extracellular fluid leading to edema and transependymal migration of liquor.

Wirth [10] have considered three different geometries of the brain: one-dimensional spherically symmetric, two-dimensional cylindrically symmetric, and three-dimensional geometry without any symmetry. The model [10] uses a nonlinear and deformation-dependent permeability function. In addition, the right side of the equations describes the source or sink of CSF in the brain parenchyma. This model can be used to evaluate the distributions of pressure, stress, and other important biophysical parameters in brain matter.

Levine [29] investigated the role of CSF absorption by the brain parenchyma. Smillie et al. [11] used a poroelastic model of the brain parenchyma combined with a hydrodynamic model of CSF. In [12], the evolution of hydrocephalus was studied using both axisymmetric and fully three-dimensional poroelastic models.

A drawback of the above models is that they do not take into account the interaction of the vascular network of the brain, parenchyma, and CSF, whereas the study of this interaction began as long ago as in the 18th century, when the Monroe–Kelly doctrine was formulated. According to this doctrine, the enclosed intracranial space contains brain matter, blood, and CSF, which occupy 80–85, 6–8, and 5–15%, respectively, of the intracranial space [30, 31]. An increase in the volume of any of these components will reduce the volume of one or two remaining components.

The first model of the Monroe intracranial cavity (compartmental model) assumed the presence of two compartments: the brain and blood. In [32, 33], this model was expanded by separately considering the arteries, capillaries, veins, venous sinuses, jugular bulb, and CSF. Further to refine the model, Sorerk et al. [32, 33] supplemented it with an additional component—brain tissue. Marmarou [34] proposed a mathematical compartmental model which is widely used to describe the dynamics of intracranial pressure. Despite the fact that this model does not explicitly take into account the vascular network of the brain or porous parenchyma, it correlates well with experimental data.

Linninger [24] proposed a complex model of the human intracranial dynamics, including the blood, CSF, brain parenchyma, and spinal canal. The model is a system of ordinary differential equations and provides transitions from normal dynamics to the diseased state. However, this model is difficult to implement.

Tully and Ventikos [35] studied fluid transport in the cerebral environment in a simplified spherically symmetric geometry using poroelastic theory (Fig. 3). This approach has made it possible to study in detail spatio–temporal fluid flow between the vascular network, CSF and the brain parenchyma and to consider hypotheses describing the onset and progression of acute and chronic hydrocephalus.

The present model three-dimensional multicomponent poroelastic model was developed by Vardakis et al. [36]. The geometry of the brain was constructed using MRI images of the brain of real patients and personalized blood flow values in inlet arteries. This model is used to evaluate two biomarkers (edema and drainage) in the early stages of Alzheimer's disease.

Several studies of hydrocephalus have examined approaches alternative to the poroelastic approach. For example, in modeling [13] of hydrocephalus and the results of shunting used for its treatment, the brain tissue is considered viscoelastic. Idealized spherically symmetric brain geometry is used: the ventricles are hollow concentric space filled with CSF. In [15], the development of hydrocephalus is also studied using a viscoelastic model of the brain parenchyma, but the brain geometry is simplified to idealized cylindrical geometry. In [14], a quasilinear viscoelastic constitutive equation for brain matter is considered using idealized cylindrical geometry. This model has been used to determine decompression and the resulting ventricular contraction after shunt placement.

It should be noted that there are generalizations of poroviscoelastic models, mostly made in [37–40]. Unlike most studies using numerical simulation, in [37–40], analytical expressions for pressure and strain are obtained under the assumption of simplified geometry.

3. INVESTIGATION OF THE POROELASTIC MODEL IN THE PARAMETER SPACE

Since a characteristic sign of hydrocephalus is ventricular deformation, it is of interest to study the influence of model parameters on the change in ventricular size and pressure for all four pore fluids at the ventricular boundary. For this, we use a two-dimensional model similar to the model of [35].

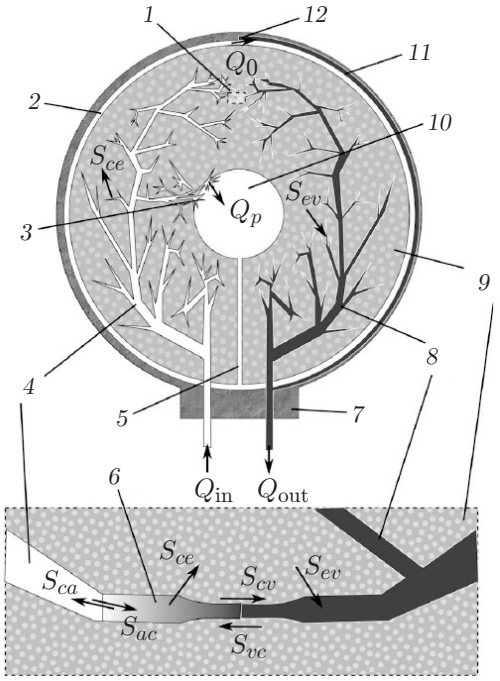

Fig. 3. Diagram of cerebral water transport in a multi-network poroelastic model [35]: (*1*) capillary exchange; (*2*) subarachnoid space; (*3*) vascular plexus; (*4*) arterial pool; (*5*) Sylvian aqueduct; (*6*) capillary pool; (*7*) skull; (*8*) venous pool; (*9*) brain tissue saturated with CSF; (*10*) ventricles; (*11*) sagittal sinus; (*12*) arachnoid granulation.

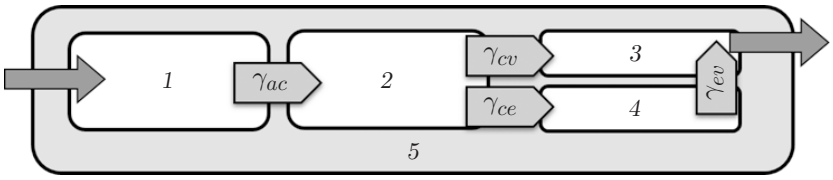

Fig. 4. Diagram of blood and CSF transfer in the brain parenchyma: (*1*) arterial pool; (*2*) capillary pool; (*3*) venous pool; (*4*) liquor pool; (*5*) parenchyma.

It is assumed that the porous matrix is the brain parenchyma, and the communicating fluid phases are the arterial (quantities with subscript a), capillary (quantities with subscript c), venous (quantities with subscript v), and liquor (quantities with subscript e) pools. Fluid exchange between the pools is shown in Fig. 4. This model takes into account the distribution and mutual influence of pressures in the pools under consideration. The mutual influence of the displacement of brain matter and these pressures is also taken into account.

The geometry of the poroelastic brain parenchyma is considered in a cylindrical approximation. The radius of the outer boundary Γ_S is r_S, and the radius of the inner boundary Γ_V (cerebral ventricles) is r_V (Fig. 5). The equilibrium equation for brain matter has the form

$$\mu\Delta\boldsymbol{u} + (\mu+\lambda)\nabla(\operatorname{div}\boldsymbol{u}) - (\alpha_a\nabla p_a + \alpha_c\nabla p_c + \alpha_e\nabla p_e + \alpha_v\nabla p_v) = 0. \tag{1}$$

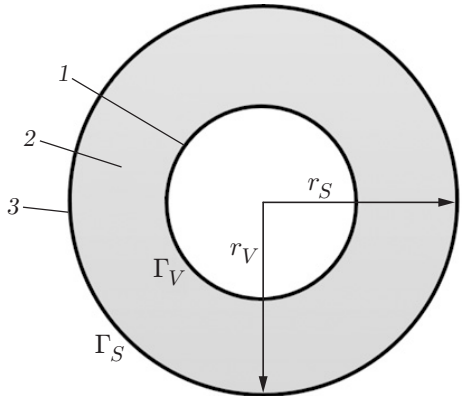

Fig. 5. Simplified parenchyma geometry: (*1*) ventricles; (*2*) parenchyma; (*3*) skull.

Using the law of conservation of mass and Darcy's law for the pore fluids, we obtain the equations

$$-(k_a/\mu_a)\,\Delta p_a + |\dot{s}_{a\to c}| = 0; \tag{2}$$

$$-(k_c/\mu_c)\,\Delta p_c - |\dot{s}_{a\to c}| + |\dot{s}_{c\to e}| + |\dot{s}_{c\to v}| = 0; \tag{3}$$

$$-(k_e/\mu_e)\,\Delta p_e - |\dot{s}_{c\to e}| + |\dot{s}_{e\to v}| = 0; \tag{4}$$

$$-(k_v/\mu_v)\,\Delta p_v - |\dot{s}_{c\to v}| - |\dot{s}_{e\to v}| = 0. \tag{5}$$

In Eqs. (1)–(5), $\boldsymbol{u}$ is the displacement of brain matter, λ and μ are the elastic moduli, p_i is the pore fluid pressure, α_i is the Biot coefficient, k_i is the permeability, and μ_i is the viscosity of the pore fluids; $i = a, c, v, e$. Unidirectional fluid flow from the network x to the network y is due to a hydrostatic pressure gradient:

$$\dot{s}_{y\to x} = -\gamma_{yx}[p_x - p_y]. \tag{6}$$

System (1)–(5) is supplemented by boundary conditions for the displacement and four pore pressures. On the cerebral ventricular boundary Γ_V, the following conditions are specified.

1. Stresses are assumed to be continuous:

$$2\mu\varepsilon(\boldsymbol{u})\cdot\boldsymbol{n} + \lambda\epsilon(\boldsymbol{u})\boldsymbol{n} = \sum_{i=a,c,e,v}(\alpha_i - 1)p_i\boldsymbol{n} \tag{7}$$

[$\varepsilon(\boldsymbol{u})$ is the strain tensor, $\epsilon(\boldsymbol{u}) = \operatorname{tr}\varepsilon(\boldsymbol{u}) = \varepsilon(\boldsymbol{u})_{ii} = \operatorname{div}\boldsymbol{u}$, and $\boldsymbol{n}$ is the outward unit normal vector].

2. For the arterial and venous networks, there is no flow:

$$\nabla p_a\boldsymbol{n} = \nabla p_v\boldsymbol{n} = 0. \tag{8}$$

3. CSF is secreted at a constant rate Q_p in the cerebral ventricles. The mass conservation condition for fluid in the ventricular system takes into account the volume of CSF produced by the vascular plexuses, the volume of CSF that seeps through the ventricular wall, and the CSF flow through the Sylvian aqueduct:

$$Q_p = \frac{\pi d^4}{128\mu L}\,(p_e\Big|_{\Gamma_V} - p_e\Big|_{\Gamma_S}) - \oint\limits_{\Gamma_V}\Big(-\frac{k_e}{\mu_e}\,\nabla p_e\Big)\cdot\boldsymbol{n}\,dS \tag{9}$$

(d and L are the diameter and length of the Sylvian aqueduct).

4. The formation of CSF from the blood leads to a drop in pressure in the network of capillaries:

$$\varkappa_{cv}\nabla p_c\boldsymbol{n} = Q_p, \tag{10}$$

where $\varkappa_{cv}$ is the resistance of the flow penetrating from the capillary network into the ventricles through the vascular plexuses.

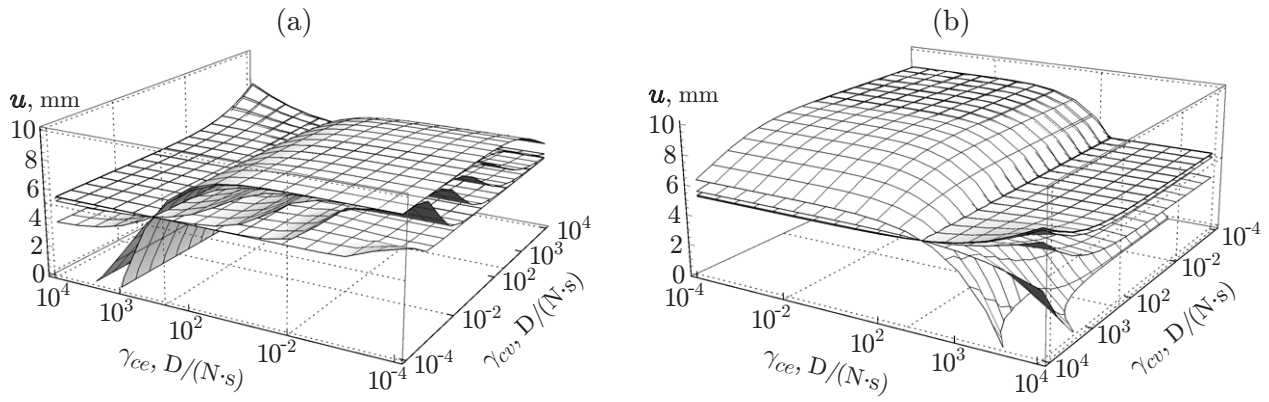

Fig. 6. Dependence of the displacement of the ventricular wall on the increasing (a) and decreasing (b) parameters γ_{ce} and γ_{cv} and $\gamma_{ev} = 100$ D/(N · s) and $\gamma_{ac} = 0.00068$, 0.1489, 3.8154, 38.2225, 231.567, 1063.08, and 4531.31.

The following assumptions are made at the boundary of the skull Γ_S.

1. Since in this paper we consider the adult human brain, the skull is considered rigid. Thus, the displacements of the skull boundary are zero:

$$\boldsymbol{u} = 0. \tag{11}$$

2. Capillary flow at the skull boundary is absent:

$$\nabla p_c \, \boldsymbol{n} = 0. \tag{12}$$

3. The arterial and venous pressures are specified:

$$p_a = p_{\text{art}}, \qquad p_v = p_{\text{ven}}. \tag{13}$$

4. The absorption of liquor into the venous network leads to an increase in pressure:

$$p_e = p_v + \mu_e R Q_0, \tag{14}$$

where R is the resistance due to the presence of arachnoid granulation and Q_0 is the CSF flow into the venous network.

It should be noted that two-dimensional models are fairly widely used to study CSF dynamics [19, 41]. Such models are simple and allow the study of the behavior of pore pressures and deformation of brain matter.

The model presented here depends on eight parameters: the four Biot coefficients α_a, α_c, α_v, and α_e corresponding to the four pore fluids and the four parameters γ_{ac}, γ_{cv}, γ_{ce}, and γ_{ev} determining the interaction of pressures in pore fluids (see Fig. 4). The range of parameter values is selected as follows: γ_{ac}, γ_{cv}, γ_{ce}, and γ_{ev} take values 10^{-4}–10^4 D/(N · s) (D denotes darcy). This range includes the physiologically sound parameter values given in [35]. The Biot coefficient are selected equal to 0.99, so that all pore fluids make equal contributions to the deformation of brain matter. For smaller values of the Biot coefficients, there are very large deformations of brain matter with a slight change in pressure.

To analyze the influence of the parameters, we constructed numerical solutions of system (1)–(14) for various values of the parameters γ_{ac}, γ_{cv}, γ_{ce}, and γ_{ev} and fixed values of the Biot coefficients. The calculation was carried out using an explicit Runge–Kutta method with an automatic choice of the integration step and the order of the method. Each of the parameters γ_{ac}, γ_{cv}, γ_{ce}, and γ_{ev} independently took values from a 15-element set covering the entire range of significant parameters: 0.0001, 0.00068, 0.0149, 0.1489, 0.8872, 3.8154, 13.1054, 38.2225, 98.5754, 231.567, 507.698, 1063.08, 2181.07, 4531.31, and 10 000.

Thus, 15^4 variants were calculated. The results of these calculations are given in interpolated form.

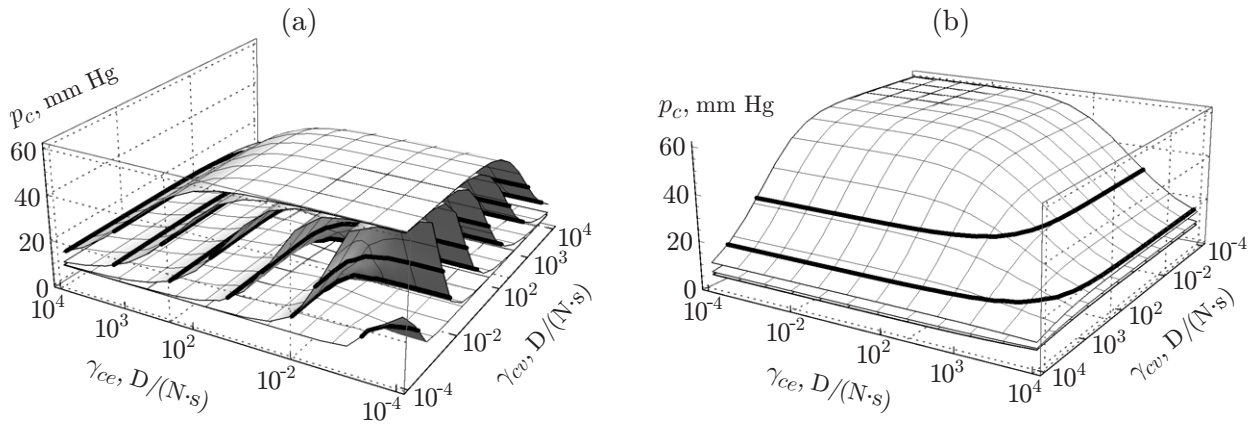

Fig. 7. Dependence of capillary pressure on the increasing (a) and decreasing (b) parameters γ_{ce} and γ_{cv} for $\gamma_{ev} = 100$ D/(N · s) and $\gamma_{ac} = 0.00068$, 0.1489, 3.8154, 38.2225, 231.567, 1063.08, and 4531.31.

3.1. Displacement of the Ventricular Wall

Figure 6 shows the dependence of the displacement of the ventricular wall on the parameters γ_{ac}, γ_{ce}, and γ_{cv} for $\gamma_{ev} = 100$ D/(N · s). Different surfaces correspond to different values of γ_{ac}. The parameter γ_{ac} takes values of 0.00068, 0.1489, 3.8154, 38.2225, 231.567, 1063.08, and 4531.31, with larger values of γ_{ac} corresponding to surfaces with larger displacements $\boldsymbol{u}$ for $\gamma_{ce} = 0$ and $\gamma_{cv} = 0$. It should be noted that the values of the parameter $\gamma_{ev} = 10^{-4}$–10^3 D/(N · s) practically do not influence the ventricular displacement. For larger values of γ_{ev}, the displacement begins to grow, increasing for $\gamma_{ev} = 10^4$ D/(N · s) by 3.5 mm. The nature of the dependences remains unchanged.

Note that along the axis of the parameter γ_{ce} in the range $\gamma_{ce} = 10^2$–10^3 D/(N · s), the character of the dependence changes and it is divided into two qualitatively different regions (see Fig. 6). In the region of small values of γ_{ce}, the ventricular displacements are large enough, which is not consistent with the physiological norm. Small displacements of the ventricle are observed only for large values of γ_{ce} and for $\gamma_{ac} > 100$ D/(N · s). In this region, there is a displacement of the ventricular wall within the physiological norm $\boldsymbol{u} \leqslant 2$ mm [22]. The parameter γ_{cv} begins to influence ventricular displacement for $\gamma_{cv} > 100$ D/(N · s). Thus, for all parameters, the range $\gamma_{cv} = 10^2$–10^3 D/(N · s) is the region of transition outside of which the parameters differently influence the displacement.

3.2. Pressure on the Ventricular Wall

Figure 7 shows the dependence of capillary pressure on the parameters γ_{ce}, γ_{cv}, and γ_{ac}. As before, the values of the parameter γ_{ac} in Fig. 6 correspond to different surfaces, with the larger values of γ_{ac} corresponding to the surfaces located higher. It should be noted that the values of the parameter γ_{ev} has practically no effect on capillary pressure. The highest capillary pressure values are achieved for small values of the parameters γ_{ce} and γ_{cv} (see Fig. 7). The pressure decreases with an increase in any of these parameters. A significant pressure reduction is observed for $\gamma_{ce} = 10^2$–10^3 D/(N · s) and $\gamma_{cv} = 10^2$–10^3 D/(N · s). The physiological norm for capillary pressure is 15–30 mm Hg. (In Fig. 7, this pressure range is indicated by bold lines). The remaining pressures, namely, the arterial, venous, and cerebrospinal fluid pressures, at the ventricular boundary remain approximately constant in the entire range of parameters and are $p_a = 60.15$ mm Hg, $p_v = 4.88$ mm Hg, and $p_e = 8.18$ mm Hg, respectively. The scatter of these pressures does not exceed 0.01 mm Hg. The values correspond to the physiological norm [42].

3.3. Range of the Physiological Norm

In a healthy person, the walls of the ventricles are displaced by no more than 2 mm, in accordance with the physiological norm. The physiological norm for capillary pressure is 15–30 mm Hg. Figure 8 shows the constant pressure surfaces $p_c = 15$ mm Hg and $p_c = 30$ mm Hg and the constant displacement surfaces at $\boldsymbol{u} = 0$; 2 mm in

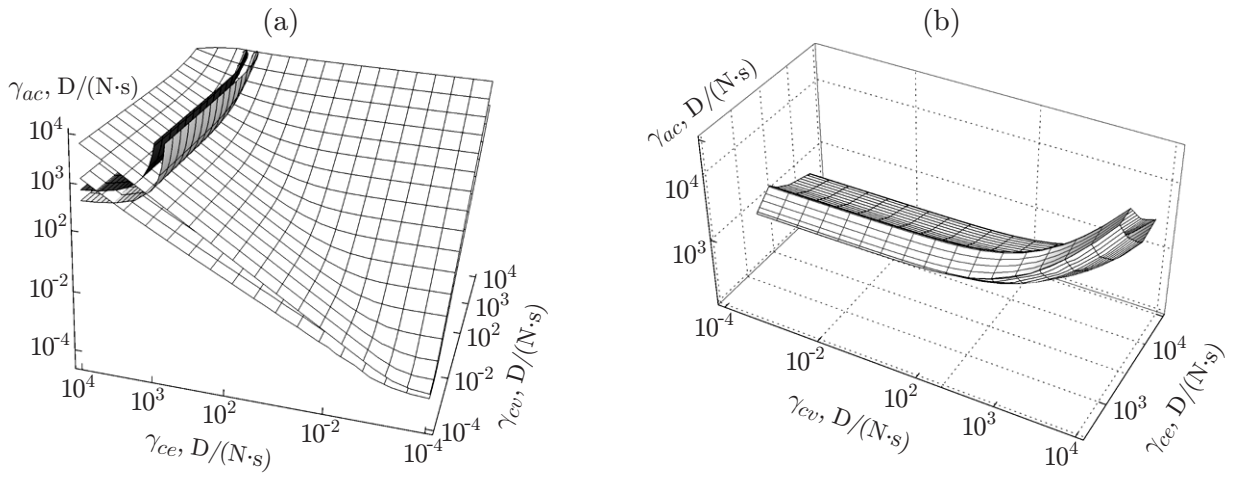

Fig. 8. Constant pressure surfaces (white) and displacements (gray) in the space of the parameters γ_{ce}, γ_{cv}, and γ_{ac} (a) and the range of the physiological norm (b).

the space of the parameters γ_{ce}, γ_{cv}, and γ_{ac}. It can be seen that these surfaces bound a region in the parameter space in which the pressure and displacement are within the normal limits (Fig. 8b). For larger γ_{ev}, this region is shifted toward larger γ_{ce} within the same order of magnitude.

3.4. Influence of Biot Coefficients

Biot coefficients are included in system (1)–(14) in a symmetric manner and uniformly affect the displacement of the ventricular wall and pressure. As the Biot coefficients decrease, the ventricular wall displacement increases and the capillary pressure decreases. The Biot coefficients have a similar effect on the other pressures. The dependence of ventricular wall displacement and pressure on the Biot coefficients is almost linear.

4. RESULTS AND DISCUSSION

The mathematical model (1)–(14) takes into account the essential pathophysiological features of hemo- and liquor dynamics. The parameter values from the region considered provides a description of the interaction of the fluids of the central nervous system in the norm and pathology.

A decrease in the parameter γ_{ce} implies a weakening of the mutual influence of capillary blood and liquor flows, which may correspond to an attenuation of the transfer pulsation, resulting in liquor retention in the cerebral ventricles and hence an increase in ventricular wall displacement (see Fig. 6). The impairment of capillary outflow leads to an increase in capillary pressure (see Fig. 7).

An increase in the parameter γ_{ac} implies an increase in the mutual influence of the arterial and capillary components, leading to the correct distribution of the pulse wave from the arterial to the capillary component, and corresponds to small displacements of the ventricular wall (see Fig. 6). A decrease in γ_{ac} indicates an impairment of arterial-capillary flow and leads to a decrease in capillary pressure and a significant displacement of the ventricular wall.

As the parameter γ_{cv} increases, there is an increase in the mutual influence of the capillary and venous components, resulting in overload of the venous component and an increase in its influence on the liquor component. As a result, the displacement of the ventricular wall increases (see Fig. 6). An increase in the parameter γ_{cv} may correspond to increased capillary outflow, which leads to a decrease in capillary pressure (see Fig. 7).

It should be noted that the brain has large compensatory capabilities, and fluctuations in real physiological parameters do not always lead to a change in its functioning. A change in the parameter γ_{cv} also influences the pressure and displacement of the ventricular wall only at large values, which correlates with the physiological characteristics of the central nervous system.

CONCLUSIONS

The proposed model can be used to describe the condition of the body both in the functional norm and in hydrocephalus and the transition between them with a change in model parameters. The model qualitatively describes the real mechanisms of hemoliquorodynamics.

We are grateful to A. P. Chupakhin for attention to this work.

This work was supported by the Russian Science Foundation (Grant No. 17-11-01156).

REFERENCES

1. D. Enzmann, N. Pelc, and J. Norbert, "Brain Motion: Measurement with Phase-Contrast MR Imaging," Radiology **185** (3), 653–660 (1992).
2. D. Enzmann, N. Pelc, and J. Norbert, "Cerebrospinal Fluid Flow Measured by Phase-Contrast Cine MR," Amer. J. Neuroradiol. **14** (6), 1301–1307 (1993).
3. A. V. Boiko, A. E. Akulov, A. P. Chupakhin, et al., "Measurement of Viscous Flow Velocity and Flow Visualization Using Two Magnetic Resonance Imagers," Prikl. Mekh. Tekh. Fiz. **58** (2), 26–31 (2017) [J. Appl. Mech. Tech. Phys. **58** (2), 209–213 (2017)].
4. G. Agarwal, B. Berman, and L. Stark, "A Lumped Parameter Model of the Cerebrospinal Fluid System," IEEE Trans. Biomed. Eng., No. 1, 45–53 (1969).
5. T. Takemae, Y. Kosugi, J. Ikebe, et al., "A Simulation Study of Intracranial Pressure Increment Using an Electrical Circuit Model of Cerebral Circulation," IEEE Trans. Biomed. Eng., No. 12, 958–962 (1987).
6. N. Alperin, E. M. Vikingstad, B. Gomez-Anson, and D. N. Levin, "Hemodynamically Independent Analysis of Cerebrospinal Fluid and Brain Motion Observed with Dynamic Phase Contrast MRI," Magn. Res. Med. **35** (5), 741–754 (1996).
7. M. Ursino, "A Mathematical Study of Human Intracranial Hydrodynamics. 1. The Cerebrospinal Fluid Pulse Pressure," Annals Biomed. Eng. **16** (4), 379–401 (1988).
8. M. Ursino, "A Mathematical Study of Human Intracranial Hydrodynamics. 2. Simulation of Clinical Tests," Annals Biomed. Eng. **16** (4), 403–416 (1988).
9. T. Nagashima, N. Tamaki, S. Matsumoto, et al., "Biomechanics of Hydrocephalus: A New Theoretical Model," Neurosurgery **21** (6), 898–904 (1987).
10. B. Wirth, *A Mathematical Model for Hydrocephalus: Master of Science in Mathematical Modelling* (Univ. of Oxford, Oxford, 2005).
11. A. Smillie, I. Sobey, and Z. Molnar, "A Hydroelastic Model of Hydrocephalus," J. Fluid Mech. **539**, 417–443 (2005).
12. B. Wirth and I. Sobey, "An Axisymmetric and Fully 3d Poroelastic Model for the Evolution of Hydrocephalus," Math. Med. Biol. **23** (4), 363–388 (2006).
13. A. Mehrabian and Y. Abousleiman, "General Solutions to Poroviscoelastic Model of Hydrocephalic Human Brain Tissue," J. Theor. Biol. **291**, 105–118 (2011).
14. C. Drapaca, G. Tenti, K. Rohlf, and S. Sivaloganathan, "A Guasi-Linear Viscoelastic Constitutive Equation for the Brain: Application to Hydrocephalus," J. Elasticity. **85** (1), 65–83 (2006).
15. K. Wilkie, C. Drapaca, and S. Sivaloganathan, "Aging Impact on Brain Biomechanics with Applications to Hydrocephalus," Math. Med. Biol. **29** (2), 145–161 (2012).
16. E. E. Jacobson, D. F. Fletcher, M. K. Morgan, and I. H. Johnston, "Fluid Ddynamics of the Cerebral Aqueduct," Pediatr. Neurosurgery **24** (5), 229–236 (1996).
17. V. Kurtcuoglu, D. Poulikakos, and Y. Ventikos, "Computational Modeling of the Mechanical Behavior of the Cerebrospinal Fluid System," J. Biomech. Eng. **127** (2), 264–269 (2005).
18. S. Gupta, M. Soellinger, P. Boesiger, et al., "Three-Dimensional Computational Modeling of Subject-Specific Cerebrospinal Fluid Flow in the Subarachnoid Space," J. Biomech. Eng. **131** (2), 021010 (2009).
19. N. Masoumi, F. Framanzad, B. Zamanian, et al., "2d Computational Fluid Dynamic Modeling of Human Ventricle System Based on Fluid-Solid Interaction and Pulsatile Flow," Basic Clin. Neurosci. **4** (1), 64–75 (2013).
20. J. Apura, J. Tiago, A. Bugalho de Moura, et al., "The Effect of Ventricular Volume Increase in the Amplitude of Intracranial Pressure," Comput. Meth. Biomech. Biomed. Eng. **22** (9), 1–12 (2019).

21. H. Benveniste, H. Lee, and N. D. Volkow, "The Glymphatic Pathway: Waste Removal from the CNS Via Cerebrospinal Fluid Transport," Neuroscientist **23** (5), 454–465 (2017).
22. I. Johnston and C. Teo, "Disorders of CSF Hydrodynamics," Child's Nervous System **16** (1011), 776–799 (2000).
23. M. Ursino and C. A. Lodi, "A Simple Mathematical Model of the Interaction between Intracranial Pressure and Cerebral Hemodynamics," J. Appl. Physiol. **82** (4), 1256–1269 (1997).
24. A. A. Linninger, M. Xenos, B. Sweetman, et al., "A Mathematical Model of Blood, Cerebrospinal Fluid and Brain Dynamics," J. Math. Biol. **59** (6), 729–759 (2009).
25. M. Sharan and A. S. Popel, "A Compartmental Model for Oxygen Transport in Brain Microcirculation in the Presence of Blood Substitutes," J. Theor. Biology. **216** (4), 479–500 (2002).
26. S. Sivaloganathan, G. Tenti, and J. Drake, "Mathematical Pressure Volume Models of the Cerebrospinal Fluid," Appl. Math. Comput. **94** (23), 243–266 (1998).
27. S. Hakim, "Biomechanics of Hydrocephalus," Acta Neurologica Latinoamericana **1**, 169–194 (1971).
28. A. Pena, M. D. Bolton, H. Whitehouse, and J. D. Pickard, "Effects of Brain Ventricular Shape on Periventricular Biomechanics: A Finite-Element Analysis," Neurosurgery **45** (1), 107–118 (1999).
29. D. N. Levine, "The Pathogenesis of Normal Pressure Hydrocephalus: A Theoretical Analysis," Bull. Math. Biology. **61** (5), 875–916 (1999).
30. A. Monro, *Observations on the Structure and Functions of the Nervous System* (William Creech, London, 1783).
31. G. Kellie, "An Account with Some Reflections on the Pathology of the Brain," Edinburgh Med. Surgic. J. **1**, 84–169 (1824).
32. S. Sorek, M. Feinsod, and J. Bear, "Can NPH be Caused by Cerebral Small Vessel Disease," Med. Biol. Eng. Comput. **26** (3), 310–313 (1988).
33. S. Sorek, J. Bear, and Z. Karni, "Resistances and Compliances of a Compartmental Model of the Cerebrovascular System," Annals Biomed. Eng. **17** (1), 1–12 (1989).
34. A. Marmarou, K. Shulman, and R. M. Rosende, "A Nonlinear Analysis of the Cerebrospinal Fluid System and Intracranial Pressure Dynamics," J. Neurosurgery **48** (3), 332–344 (1978).
35. B. Tully and Y. Ventikos, "Cerebral Water Transport Using Multiple-Network Poroelastic Theory: Application to Normal Pressure Hydrocephalus," J. Fluid Mech. **667**, 188–215 (2011).
36. J. C. Vardakis, L. Guo, T. W. Peach, et al., "Fluid-Structure Interaction for Highly Complex, Statistically Defined, Biological Media: Homogenisation and a 3d Multi-Compartmental Poroelastic Model for Brain Biomechanics," J. Fluids Struct. **91** (102641), 1–16 (2019).
37. G. Tenti, J. Drake, and S. Sivaloganathan, "Brain Biomechanics: Mathematical Modeling of Hydrocephalus," Neurolog. Res. **22** (1), 19–24 (2000).
38. G. Tenti, S. Sivaloganathan, and J. M. Drake, "Brain Biomechanics: Steady-State Consolidation Theory of Hydrocephalus," Canad. Appl. Math. Quart. **7** (1), 93–110 (1999).
39. S. Sivaloganathan, M. Stastna, G. Tenti, and J. Drake, "A Viscoelastic Model of the Brain Parenchyma with Pulsatile Ventricular Pressure," Appl. Math. Comput. **165** (3), 687–698 (2005).
40. S. Sivaloganathan, M. Stastna, G. Tenti, and J. M. Drake, "A Viscoelastic Approach to the Modelling of Hydrocephalus," Appl. Math. Comput. **163** (3), 1097–1107 (2005).
41. S. Cheng, E. Jacobson, and L. Bilston, "Models of the Pulsatile Hydrodynamics of Cerebrospinal Fluid Flow in the Normal and Abnormal Intracranial System," Comp. Meth. Biomech. Biomed. Eng. **10** (2), 151–157 (2007).
42. C. E. Johanson, J. A. Duncan, P. M. Klinge, et al., "Multiplicity of Cerebrospinal Fluid Functions: New Challenges in Health and Disease," Cerebrospinal Fluid Res. **5** (1), 1–32 (2008).